Two Hundred Fifty Years of Reconstructed South Asian Summer Monsoon Intensity and Decadal-Scale Variability

Sean P. Bryan[1,2] iD, Konrad A. Hughen[1] iD, Kristopher B. Karnauskas[3,4] iD, and J. Thomas Farrar[5] iD

[1]Department of Marine Chemistry and Geochemistry, Woods Hole Oceanographic Institution, Woods Hole, MA, USA, [2]Now at Department of Geosciences, Colorado State University, Fort Collins, CO, USA, [3]Cooperative Institute for Research in Environmental Sciences, University of Colorado Boulder, Boulder, CO, USA, [4]Department of Atmospheric and Oceanic Sciences, University of Colorado Boulder, Boulder, CO, USA, [5]Department of Physical Oceanography, Woods Hole Oceanographic Institution, Woods Hole, MA, USA

Abstract Climate model simulations of the summer South Asian monsoon predict increased rainfall in response to anthropogenic warming. However, instrumental data show a decline in Indian rainfall in recent decades, underscoring the critical need for additional, independent records of past monsoon variability. Here, we present new reconstructions of annual summer South Asian Monsoon circulation over the past 250 years, based on the geochemical barium-calcium signature of dust present in Red Sea corals. These records reveal how monsoon circulation has evolved with warming climate and indicate a significant multi-century long monsoon intensification, with decreased multidecadal variance. Stronger monsoon circulation would have increased the moisture transport from the Arabian Sea and Bay of Bengal over the Indian subcontinent. If these trends continue, the monsoon circulation and associated moisture transport and precipitation will remain strong and stable for several decades.

Plain Language Summary Despite the importance of the summer South Asian monsoon in controlling the timing and amount of precipitation delivered to more than a billion people across South Asia, there remains considerable uncertainty in how the monsoon system has changed as climate has warmed over the past couple centuries. Understanding the past behavior of the monsoon system aids in the projection of future monsoon variability and trends. In this paper, we present new, independent reconstructions of South Asian monsoon circulation. These reconstructions are derived from the geochemistry of corals collected from the Red Sea. Winds driven by the South Asian monsoon circulation blow dust from the Tokar Gap region of Sudan, which is deposited on the Red Sea. The dust releases barium to seawater, which is then incorporated into coral skeletons. These records show a multi-century long trend of increasing monsoon intensity and weakening multidecadal-scale variability. This suggests that as the climate warmed, the monsoon circulation became stronger and more stable on multidecadal timescales. Stronger monsoon circulation would have increased the moisture transport over the Indian subcontinent, increasing precipitation. If these trends continue, we would expect the monsoon circulation and associated precipitation to remain strong and stable for several decades.

1. Introduction

The summer South Asian Monsoon (SAM) is a prominent feature of Earth's climate system, controlling the timing and amount of precipitation delivered to more than a billion people across South Asia (Webster et al., 1998). The summer SAM, or Indian Monsoon, consists of the seasonal circulation associated with the trough that develops over the Indian subcontinent during the boreal summer (Goswami et al., 2006; Webster et al., 1998), which is a component of the northward migration of the Intertropical Convergence Zone (Gadgil, 2003). The seasonal change in the winds is intimately coupled with a seasonal change in precipitation: the latent heat release during precipitation drives the winds and the convergence of moisture driven by the winds drives the precipitation (Goswami & Chakravorty, 2017). The SAM varies on a variety of timescales, from daily to multidecadal and beyond (Naidu et al., 2015; Roxy et al., 2015; Turner & Annamalai, 2012). Failure of the monsoon rains can lead to drought and famine, while excess rainfall leads to severe flooding, highlighting the importance of

understanding the mechanisms controlling SAM variability. Anthropogenic greenhouse gas forcing increases the land-sea temperature and pressure gradients over South Asia (Sutton et al., 2007), which is thought to be one driver of monsoon intensification (Turner & Annamalai, 2012; Wu et al., 2012). However, many instrumental data sets indicate a decrease in monsoon rainfall (Guhathakurta & Rajeevan, 2008; Kitoh et al., 2013; Zhou et al., 2008) and circulation (Krishnan et al., 2013; Tokinaga et al., 2012) since the 1950s. One possible explanation for this discrepancy is that precipitation is highly heterogeneous in time and space, and these results depend to some degree on the exact region and time interval, and even month or threshold of rainfall intensity being studied (Naidu et al., 2015; Turner & Annamalai, 2012). Some researchers do find increases in monsoon circulation and extreme rainfall events over the past several decades (Goswami et al., 2006; Wang et al., 2013), but a recent decrease in summer monsoon rainfall nonetheless appears to be the more common finding in instrumental records (Guhathakurta & Rajeevan, 2008; Kitoh et al., 2013; Krishnan et al., 2013; Tokinaga et al., 2012; Zhou et al., 2008). Another explanation for the discrepancy between models and observations may lie in the increase of sulfate aerosols over this period, which serve to offset the effects of warming and decrease monsoon rainfall by reflecting incoming solar radiation (Guo et al., 2016). These uncertainties underscore the need for reliable long-term records of monsoon circulation to clarify the controlling mechanisms and improve model simulations of current and future monsoon variability (Roxy et al., 2015).

Observations and mesoscale modeling of wind over the Red Sea reveal seasonal, cross-axis wind jets that routinely develop through gaps in the western coastal mountains (Jiang et al., 2009). The most prominent of these is an eastward blowing jet that develops in summer and is funneled through the Tokar Gap on the Sudanese coast (Figure 1). Gridded observations of summertime (June–August) surface wind from 1950–2010 show consistent SW winds in the Tokar Gap region associated with the large-scale SAM circulation and Intertropical Convergence Zone migration (Davis et al., 2015; Jiang et al., 2009; Vareed Joseph et al., 2013). Comparison of Tokar Jet wind speed and the Indian Monsoon Index (Wang et al., 2001) from 2000–2009 shows significant correlations for monthly mean and August-only anomaly data (Figure S1 in the supporting information; $r = 0.91$ and $r = 0.52$, $p = 0.15$, respectively (Zhai, 2011). The Tokar Gap wind jet therefore represents a novel proxy for the overall intensity of the SAM circulation. The Tokar Jet generates dust storms originating from the Baraka River delta (Goudie, 2008; Hickey & Goudie, 2007; Figure 1), which can last for several days, depositing dust onto the Red Sea (Engelbrecht et al., 2017; Kalenderski & Stenchikov, 2016) and influencing surface water chemistry (e.g., Chen et al., 2008). A record of dust input to the south central Red Sea therefore has the potential to reconstruct long-term patterns of change in Tokar Gap winds and SAM intensity. To produce such a record, we analyzed the trace element geochemistry of two long-lived *Porites* spp. corals collected at Coral Gardens and Canyon reefs off the Saudi Arabian coast across from the Tokar Gap. Specifically, we use barium-calcium ratios (Ba/Ca) in the coral skeletal aragonite, which have been previously used to reconstruct riverine sediment flux to the ocean (McCulloch et al., 2003). Fine-grained floodplain sediments that enter the Red Sea via eolian transport from the Tokar Gap are also expected to release Ba into the seawater. Barium is incorporated into coralline aragonite in proportion to seawater concentrations (Lea et al., 1989). Coral Ba/Ca, therefore, should record changes in the flux of dust through the Tokar Gap and the large-scale circulation patterns that control that flux.

2. Methods

2.1. Coral Sampling and Analysis

Massive colonies of *Porites* spp*.,* living at 3- to 5-m depths, were sampled between 2008 and 2010 from sites along a north–south transect on the eastern edge of the Red Sea. Coral cores were drilled using a 10-cm diameter underwater hydraulic drill and SCUBA. The corals were located on the southeast platform of the reefs at Coral Gardens (21.78°N, 38.83°E) and Canyon (19.89°N, 39.96°E; Figure 1).

At Woods Hole Oceanographic Institution (WHOI), cores were halved, and a 1-cm thick slab was cut from the center of the core. The coral slabs were X-rayed at Falmouth Hospital (Figures S2 and S3). These corals display annual density banding and linear growth rates of 1 to 1.5 cm/year, providing precise age models. The Coral Gardens core covers the time period from 1771–2008, and the Canyon core covers 1761–2009. Approximately 15 years of high-resolution (approximately biweekly) samples were drilled at 0.5-mm
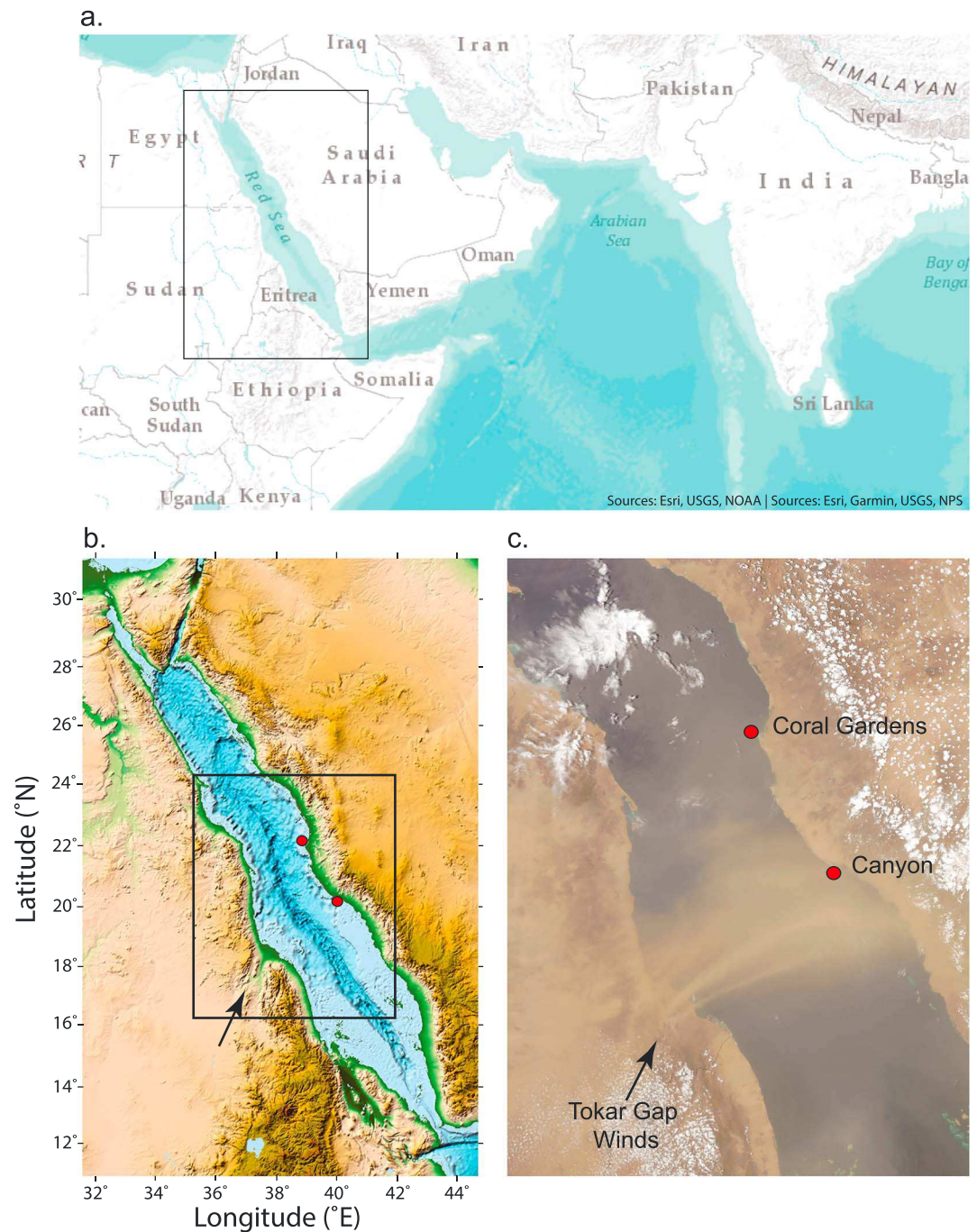
Figure 1. Geographic context of the Red Sea study area. (a) Regional map showing the study area. The black rectangle shows the area covered in (b). Map was created in ArcGIS online (https://www.arcgis.com). (b) Combined topographic and bathymetric map (ETOPO1 Global Relief Model) shows locations of coral cores as red dots. Shading indicates elevation and depth, and the black rectangle shows the area covered by the satellite photo in (c). The Tokar Gap is indicated by the arrow. (c) NASA MODIS satellite image taken 26 July 2012 shows a dust plume originating from the Tokar Gap. The locations of Canyon and Coral Gardens reefs are indicated by red circles. NASA = National Aeronautics and Space Administration; MODIS = Moderate Resolution Imaging Spectroradiometer.

increments from each coral core using a dental drill bit affixed to a drill press. Care was taken to align the drill path parallel to the axis of coral growth. Each sample consisted of ~250 μg of coral powder. Low-resolution (annual) samples were cut from the slabs using a diamond-coated cutoff wheel attached to a Dremel tool for the entire length of the coral cores. X-rays were overlain on the coral slabs to visually

identify annual layers. Annual samples were chemically cleaned using a procedure based on methods described in Shen and Boyle (1988) (supporting information Text S1). Chemical cleaning removes any nonlattice-bound trace elements, isolating the dissolved seawater [Ba] signal. The high-resolution samples were not chemically cleaned and as such may include potential signals from particulate or adsorbed phases.

All samples were dissolved in 5% nitric acid (Optima grade) and analyzed for trace and minor element concentrations by inductively coupled plasma mass spectrometry on a Thermo Element 2. Coral Gardens high-resolution, drilled samples were analyzed at the University of Colorado Institute of Arctic and Alpine Research. All other samples were analyzed at the WHOI Plasma Mass Spectrometry Facility. Annual samples were diluted to ~80-ppm Ca to avoid matrix-related effects, although tests revealed no significant matrix effects for Ba/Ca or Sr/Ca. Samples were run in a randomized order, with a blank and standards every eight samples. Elemental intensity ratios were converted to molar ratios using standard curves consisting of gravimetrically prepared multielement standards. An in-house coral powder standard (Bunaken Coral Powder) was analyzed as part of each run to monitor long-term consistency; relative standard deviations over the course of all runs was 2.4% for Ba/Ca and 0.54% for Sr/Ca. Long-term instrumental or standard solution drift was monitored and corrected using the Bunaken Coral Powder standard.

2.2. Red Sea Dust as a Barium Source

We confirm that dust deposited on the Red Sea is a significant source of labile Ba, which can readily dissolve in seawater, by experimental addition of dust collected near the coral locations to filtered seawater. Dust was collected from meteorological equipment that had been deployed on the Red Sea coast north of Jeddah, Saudi Arabia, for 3 years. Varying amounts of dust were then added to high-density polyethylene bottles along with 20 ml of 0.2-μm filtered seawater from Vineyard Sound near WHOI. A sample bottle with filtered Vineyard Sound seawater with no dust added was used as a control. The bottles were placed on a shaker table for 3 weeks, after which the seawater was filtered again to remove all dust. The seawater was diluted 20 times with 5% nitric acid (Optima Grade) and analyzed for elemental concentrations (Ba, Ca, Sr, Fe, Al) by inductively coupled plasma mass spectrometry at the WHOI Plasma Mass Spectrometry Facility.

Ba, Ca, and Sr concentrations increased with increasing dust additions. Fe and Al were not significantly different from blanks for all samples. With each dust addition, [Ba] increased proportionally more than [Ca], such that the Ba/Ca ratio increases with increasing dust addition (Figure S4). In contrast, Sr/Ca decreased with increasing dust addition due to a proportionally larger increase in [Ca] than [Sr]. The relationship between seawater Ba/Ca and the amount of dust added is somewhat logarithmic, suggesting that either the solution was nearing saturation or the kinetics of cation exchange are impacted by the very high particle content in the samples with the largest dust addition. However, the eolian dust collected from the Red Sea clearly contains labile Ba that is easily released upon interaction with seawater.

X-ray diffraction analysis conducted at WHOI on the dust samples indicates the presences of quartz, gypsum, halite, calcite, and kaolinite, suggesting that Ba may be sourced from an adsorbed phase, rather than from the dissolution of Ba-rich minerals such as barite, and is released to seawater through the same ion exchange reactions that operate in estuaries (Coffey et al., 1997). However, there is some variance in the concentration of Ba between the different dust samples. The samples that have gypsum as a major mineral have higher Ba concentrations, followed by those that contain halite. One sample, which only contains quartz as a major mineral, has the lowest Ba concentrations. These results suggest that the evaporite minerals are the most likely potential Ba source.

3. Results

3.1. Coral Ba/Ca Records

High-resolution (biweekly) analysis of the two coral cores for the interval 1994–2009 shows a distinct seasonal cycle in Ba/Ca that is strongly correlated with local sea surface temperature (SST), from National Oceanic and Atmospheric Administration (NOAA) Extended Reconstructed SST version 4 (ERSST; Huang et al., 2015), and coral strontium-calcium (Sr/Ca), a known proxy for SST (Figures 2a, S5, and S6; Beck et al., 1992). A negative relationship between temperature and the incorporation of Ba into aragonite has been previously suggested for corals (Lea et al., 1989) and demonstrated in abiotic aragonite (Gaetani & Cohen, 2006). The seasonal cycle in coral Ba/Ca can best be explained by the temperature influence on Ba incorporation.
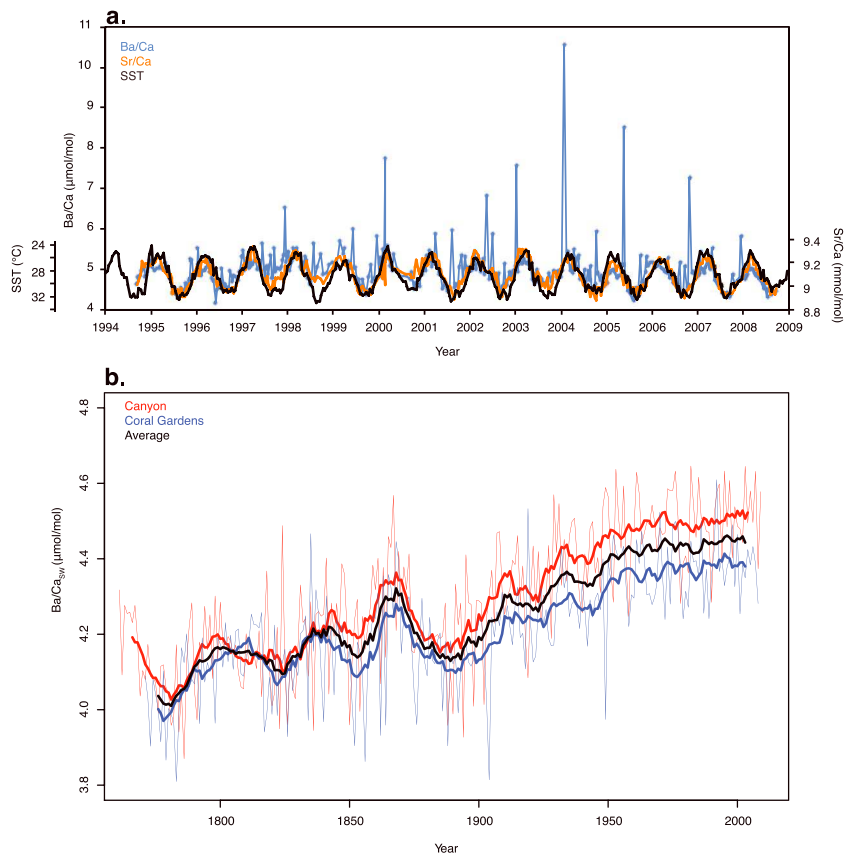
Figure 2. Tokar Gap dust signal recorded by coral skeletal barium. (a) High-resolution (biweekly) Ba/Ca (blue), Sr/Ca (orange), sea surface temperature (SST, black) data from the Coral Gardens location show Ba/Ca spikes caused by multiday dust storms superimposed on the seasonal SST cycle. (b) Annually resolved records of coral Ba/Ca with the temperature component removed for Canyon (red) and Coral Gardens (blue) locations show changes due to Ba/Ca in seawater (Ba/Ca$_{SW}$). The records reveal centennial-scale increasing trends and pronounced multidecadal variability. Thin lines are annual measurements and thick lines are 11-year running averages. The average of the two corals is shown in black (11-year average only).

Superimposed on the seasonal SST cycle are Ba/Ca peaks that reflect changes in seawater Ba/Ca due to the addition of Ba to the Red Sea by Tokar Gap dust storms (Figure 2a). Ba/Ca measured at annual resolution extends over the length of the coral cores. To isolate the changes in seawater Ba/Ca from the temperature influence in the coral cores, concurrent Sr/Ca measurements, and the observed recent Ba/Ca-Sr/Ca relationship were used to remove the temperature component from the Ba/Ca records (Figures S5 and S6 and Text S2). The resulting records of temperature-corrected Ba/Ca in seawater in the eastern Red Sea (hereafter Ba/Ca$_{SW}$) show striking agreement over the last ~250 years (Figure 2b). Both records reveal large multidecadal variability superimposed on a long-term trend and are strongly correlated at annual and decadal timescales ($r = 0.66$, $p \ll 0.0001$; and $r = 0.96$, $p \ll 0.0001$; respectively). As expected, the southern coral (Canyon) closest to the Tokar Gap dust source contains higher time mean values of Ba/Ca$_{SW}$, particularly after 1850. The close agreement to each other of these two records from sites separated by more than 200 km confirms that coral Ba/Ca$_{SW}$ is responding to a mutual large-scale climate forcing, rather than local effects.

3.2. Connection to Monsoon Circulation

To investigate the large-scale climate patterns associated with our reconstructed Red Sea dust variability, we mapped the linear regressions of gridded seasonal sea level pressure (SLP) over the period 1871–2015, using the NOAA 20th Century Reanalysis version 2 data set (Compo et al., 2011), onto the Ba/Ca$_{SW}$ indices. A coherent pattern of anomalously low pressure over the Indian subcontinent during the summer season
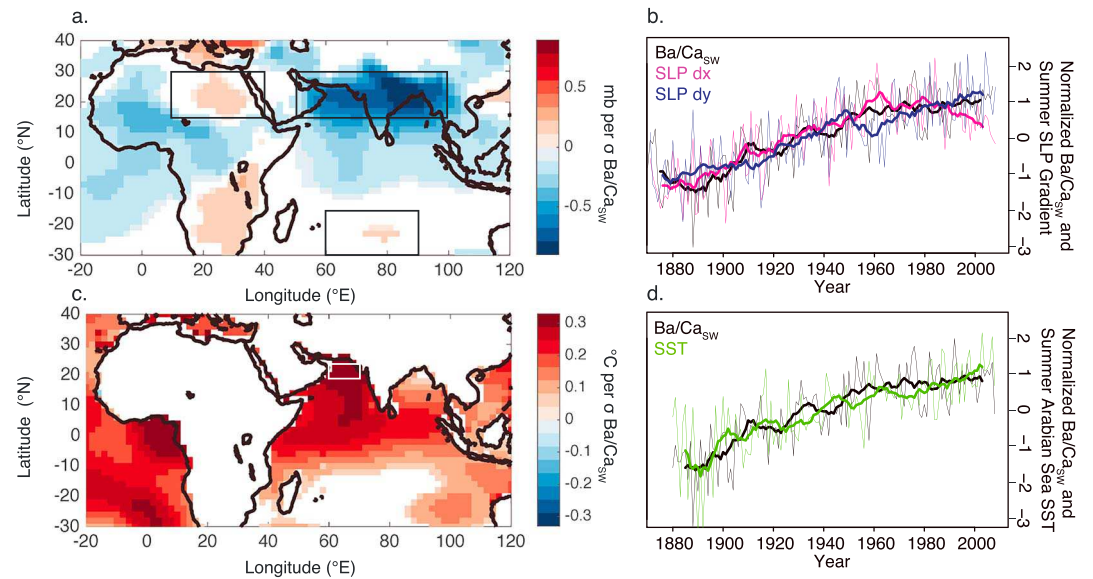
Figure 3. Comparisons of coral monsoon record with gridded climate data. (a) Regression map of summer (June–August) sea level pressure (SLP) against average of Canyon and Coral Gardens Ba/Ca$_{SW}$ for the time period 1871–2008. SLP data are from the NOAA 20C Reanalysis v2. Black boxes show the regions over which SLP is averaged to compute the zonal pressure gradient (SLP dx) and meridional pressure gradient (SLP dy) time series shown in b. (b) Normalized average Ba/Ca$_{SW}$ (black) plotted with the summer SLP gradient between North Africa and India (magenta) and summer SLP gradient between the southern Indian Ocean and India (blue). Thin lines are annual values and thick lines are 11-year running averages. (c) Regression map of summer-gridded sea surface temperature (SST) data from NOAA ERSST v4 against annual average Ba/Ca$_{SW}$ data for the period 1880–2008. The white box shows the domain used for the Arabian Sea SST index in d. (d) Same as (b), except Ba/Ca$_{SW}$ (black) is plotted with summer Arabian Sea SST (green). NOAA = National Oceanic and Atmospheric Administration; ERSST = Extended Reconstructed Sea Surface Temperature.

(June–August) is found to be associated with high Ba/Ca$_{SW}$ (representing a stronger Tokar Jet and greater dust input; Figure 3a). This reconstructed pattern is highly consistent with that of the summer SAM (Turner & Annamalai, 2012; Webster et al., 1998). Similarly, regressing gridded SST observations onto the Ba/Ca$_{SW}$ signal using NOAA ERSSTv4 (Huang et al., 2015) reveals a coherent pattern of anomalously warm summertime SST in the northern Arabian Sea (Figure 3c). To further examine these relationships between our dust reconstructions and key surface climate fields associated with the monsoon system, time series were computed for the zonal SLP gradient between South Asia and northeastern Africa, corresponding to the western transverse limb of the SAM (Webster et al., 1998), as well as the meridional SLP gradient between South Asia and the Southern Tropical Indian Ocean, corresponding to the lateral main limb of the SAM, and for northern Arabian Sea SST (Figures 3b and 3d). The Ba/Ca$_{SW}$ signal shows very strong correlations to both the zonal SLP gradient and the meridional SLP gradient ($r = 0.65$, $p \ll 0.0001$, and $r = 0.58$, $p \ll 0.0001$, respectively for annual data, and $r = 0.96$, $p \ll 0.00001$ and $r = 0.96$, $p \ll 0.0001$, respectively for decadal averages). While the correlation to the meridional SLP gradient is driven by the long-term increasing trend, the correlation to the zonal SLP gradient remains present ($r = 0.19$, $p = 0.02$) for annual data and strong ($r = 0.72$, $p \ll 0.0001$) for decadal averages when the time series are detrended. Ba/Ca$_{SW}$ is also strongly correlated to Arabian Sea summer SSTs ($r = 0.59$, $p \ll 0.0001$ for annual data and $r = 0.94$, $p \ll 0.0001$ for decadal averages). Stronger SLP gradients are indicative of stronger monsoonal and regional circulations, while warmer SST in the Arabian Sea yields greater potential for evaporative flux which supplies the monsoon with the necessary water vapor and latent heat. The strength of the Indian low pressure system together with the warmth of northern Arabian Sea SST are both fundamental and physically consistent components of the SAM dynamic circulation and thermodynamic processes. These processes are intimately linked to moisture transport and precipitation that affects the livelihoods of billions of people (Shukla & Misra, 1977). Red Sea Ba/Ca$_{SW}$ captures much of the variability in this dynamic system, particularly on decadal timescales, and therefore offers an opportunity to extend our understanding of the SAM beyond the instrumental record.
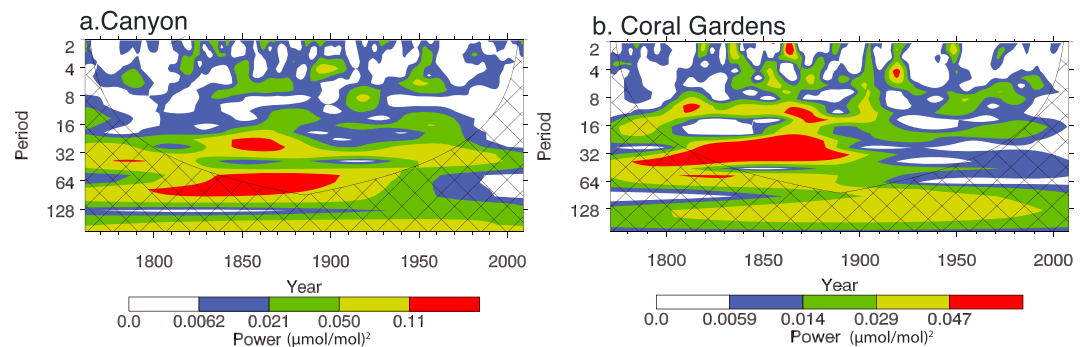
Figure 4. Evolution of South Asian Monsoon variability through time. (a) The Morlet wavelet power spectrum (Torrence & Compo, 1998) of Canyon Ba/Ca$_{SW}$ reveals decreasing multidecadal variance at 30- and 60-year periods in the recent century. The contour levels are chosen so that 75%, 50%, 25%, and 5% of the wavelet power is above each level, respectively. The cross-hatched region is the cone of influence, where zero padding has reduced the variance. (b) Same as (a), except for Coral Gardens Ba/Ca$_{SW}$.

4. Discussion: Long-Term Trends and Decadal-Scale Variability

We now turn our attention to the different timescales of variability present in the reconstructed Red Sea dust records, and their possible connections with well-known modes of large-scale climate variability. Ba/Ca$_{SW}$ shows a positive trend over the length of the record, increasing by ~10% from the end of the Little Ice Age (LIA), ~1800–1850, to the present (Figure 2). The strong regressions between Ba/Ca$_{SW}$ and India-North Africa SLP gradients for both average summer and monthly mean data (not shown) suggest that changes in Ba/Ca$_{SW}$ predominantly reflect wind strength during the summer monsoon season, rather than changes in the monsoon duration. These results are consistent with records of monsoon wind intensity based on the abundance of the upwelling indicator foraminifera *Globigerina bulloides* in Arabian Sea sediments, which show an increasing trend over the past several centuries (Anderson et al., 2002). Records of monsoon rainfall from stable isotopes in Indian speleothems also show an increase of Indian summer monsoon rainfall during the nineteenth and early twentieth centuries following LIA weakening (Sinha et al., 2015). Arabian Sea SSTs were cooler during the LIA (Boell et al., 2014), which would have helped reduce evaporation and moisture transport and therefore reduced the strength of convective rainfall. This would have acted as a positive feedback on the intensity of the cyclonic circulation over India and the transport of moisture from the Arabian Sea.

Power spectral analysis of both coral monsoon records shows prominent peaks in variance at periods of about 30 and 60 years, and minor peaks around 6 and 12 years, with the records significantly coherent and in-phase at periods of 30 years and longer (Figure S8). The variance in the records also changes through time; it is highest in the late nineteenth century and decreases throughout the twentieth century. This decline in variance occurs across the spectrum of frequencies (Figure 4) but is particularly evident at longer periods, where large multidecadal oscillations are clearly evident in the first half of the records but become muted during the twentieth century. The elevated variance near 30- and 60-year periods is reminiscent of the Atlantic Multidecadal Oscillation (AMO; Gray et al., 2004), which has been tied to monsoon variability with increased SAM rainfall during positive AMO phases (Krishnamurthy & Krishnamurthy, 2016; Zhang & Delworth, 2006). Although the coral SAM records and the AMO share 30- and 60-year periodicities of variance, the records show no coherence at these frequencies, and there is no correlation between detrended Ba/Ca$_{SW}$ and the AMO. Further, wavelet analysis shows that the multidecadal power in the AMO has increased over the past couple of centuries (Figure S9), in contrast to that of Ba/Ca$_{SW}$ which has decreased. This suggests that the AMO may contribute to pacing multidecadal variability in SAM intensity, but the relationship is either nonlinear or other forcings are more important in setting the amplitude.

5. Summary

Current GCMs struggle to capture some processes involved in monsoon variability, impacting predictions of how SAM circulation and rainfall will respond to future anthropogenic warming (Guo et al., 2016; Sutton et al., 2007). The coral Ba/Ca$_{SW}$ records presented here reveal a long-term increase in mean intensity of

the SAM during the late nineteenth and twentieth centuries, likely linked to Northern Hemisphere mean summer warming following the LIA. Although this finding contrasts with instrumental records of Indian precipitation, which show multidecadal variability but no longer-term trend (Turner & Annamalai, 2012), long-term, centennial-scale monsoon variability has also been found in previous reconstructions of SAM winds from Arabian Sea sediments (Anderson et al., 2002) and monsoon rainfall from Indian speleothems (Sinha et al., 2015). We propose that the spatial heterogeneity of instrumental precipitation records or their limited duration is masking lower-frequency signals in the spatially averaged rainfall indices. In fact, a long-term decline in SLP over the Indian subcontinent can indeed be seen in reanalysis data (Compo et al., 2011; (Figure S10), supporting the potential for long-term precipitation trends as well. Our Red Sea coral-based monsoon records also capture strong multidecadal variability, which is perhaps paced by teleconnections to the AMO. This history of multidecadal variability in the SAM circulation shows a pattern of long-term modulation suggesting that such pronounced variability may return in the future. However, this multidecadal variability in the monsoon has weakened consistently during the last century, and if the trends revealed here continue, we would expect a strong, stable SAM circulation for the next several decades.

References

Anderson, D. M., Overpeck, J. T., & Gupta, A. K. (2002). Increase in the Asian southwest monsoon during the past four centuries. *Science*, *297*(5581), 596–599. https://doi.org/10.1126/science.1072881

Beck, J., Edwards, R., Ito, E., Taylor, F., Recy, J., Rougerie, F., et al. (1992). Sea-surface temperature from coral skeletal strontium calcium ratios. *Science*, *257*(5070), 644–647. https://doi.org/10.1126/science.257.5070.644

Boell, A., Lueckge, A., Munz, P., Forke, S., Schulz, H., Ramaswamy, V., et al. (2014). Late Holocene primary productivity and sea surface temperature variations in the northeastern Arabian Sea: Implications for winter monsoon variability. *Paleoceanography*, *29*, 778–794. https://doi.org/10.1002/2013PA002579

Chen, Y., Paytan, A., Chase, Z., Measures, C., Beck, A. J., Sanudo-Wilhelmy, S. A., & Post, A. F. (2008). Sources and fluxes of atmospheric trace elements to the Gulf of Aqaba, Red Sea. *Journal of Geophysical Research*, *113*, D05306. https://doi.org/10.1029/2007JD009110

Coffey, M., Dehairs, F., Collette, O., Luther, G., Church, T., & Jickells, T. (1997). The behaviour of dissolved barium in estuaries. *Estuarine Coastal and Shelf Science*, *45*(1), 113–121. https://doi.org/10.1006/ecss.1996.0157

Compo, G. P., Whitaker, J. S., Sardeshmukh, P. D., Matsui, N., Allan, R. J., Yin, X., et al. (2011). The twentieth century reanalysis project. *Quarterly Journal of the Royal Meteorological Society*, *137*(654), 1–28. https://doi.org/10.1002/qj.776

Davis, S. R., Pratt, L. J., & Jiang, H. S. (2015). The Tokar gap jet: Regional circulation, diurnal variability, and moisture transport based on numerical simulations. *Journal of Climate*, *28*(15), 5885–5907. https://doi.org/10.1175/jcli-d-14-00635.1

Engelbrecht, J. P., Stenchikov, G., Prakash, P. J., Lersch, T., Anisimov, A., & Shevchenko, I. (2017). Physical and chemical properties of deposited airborne particulates over the Arabian Red Sea coastal plain. *Atmospheric Chemistry and Physics*, *17*(18), 11,467–11,490. https://doi.org/10.5194/acp-17-11467-2017

Gadgil, S. (2003). The Indian monsoon and its variability. *Annual Review of Earth and Planetary Sciences*, *31*(1), 429–467. https://doi.org/10.1146/annurev.earth.31.100901.141251

Gaetani, G. A., & Cohen, A. L. (2006). Element partitioning during precipitation of aragonite from seawater: A framework for understanding paleoproxies. *Geochimica et Cosmochimica Acta*, *70*(18), 4617–4634. https://doi.org/10.1016/j.gca.2006.07.008

Goswami, B., & Chakravorty, S. (2017, April 26). Dynamics of the Indian summer monsoon climate. *Oxford Research Encyclopedia of Climate Science*. Ed. Retrieved 20 Mar. 2019, from http://oxfordre.com/climatescience/view/10.1093/acrefore/9780190228620.001.0001/acrefore-9780190228620-e-613

Goswami, B. N., Venugopal, V., Sengupta, D., Madhusoodanan, M. S., & Xavier, P. K. (2006). Increasing trend of extreme rain events over India in a warming environment. *Science*, *314*(5804), 1442–1445. https://doi.org/10.1126/science.1132027

Goudie, A. S. (2008). The history and nature of wind erosion in deserts. *Annual Review of Earth and Planetary Sciences*, *36*(1), 97–119. https://doi.org/10.1146/annurev.earth.36.031207.124353

Gray, S., Graumlich, L., Betancourt, J., & Pederson, G. (2004). A tree-ring based reconstruction of the Atlantic Multidecadal Oscillation since 1567 AD. *Geophysical Research Letters*, *31*, L12205. https://doi.org/10.1029/2004GL019932

Guhathakurta, P., & Rajeevan, M. (2008). Trends in the rainfall pattern over India. *International Journal of Climatology*, *28*(11), 1453–1469. https://doi.org/10.1002/joc.1640

Guo, L., Turner, A. G., & Highwood, E. J. (2016). Local and remote impacts of aerosol species on Indian summer monsoon rainfall in a GCM. *Journal of Climate*, *29*(19), 6937–6955. https://doi.org/10.1175/JCLI-D-15-0728.1

Hickey, B., & Goudie, A. S. (2007). The use of TOMS and MODIS to identify dust source areas: The Tokar delta (Sudan) and the Seistan basin (south West Asia). In A. S. K. J. Goudie (Ed.), *Geomorphological Variations* (pp. 37–57). Prague: P3K Publishers.

Huang, B., Banzon, V. F., Freeman, E., Lawrimore, J., Liu, W., Peterson, T. C., et al. (2015). Extended reconstructed sea surface temperature version 4 (ERSST.v4) part I: Upgrades and Intercomparisons. *Journal of Climate*, *28*(3), 911–930. https://doi.org/10.1175/JCLI-D-14-00006.1

Jiang, H. S., Farrar, T., Beardsley, R. C., Chen, R., & Chen, C. S. (2009). Zonal surface wind jets across the Red Sea due to mountain gap forcing along both sides of the Red Sea. *Geophysical Research Letters*, *36*, L19605. https://doi.org/10.1029/2009GL040008

Kalenderski, S., & Stenchikov, G. (2016). High-resolution regional modeling of summertime transport and impact of African dust over the Red Sea and Arabian peninsula. *Journal of Geophysical Research: Atmospheres*, *121*, 6435–6458. https://doi.org/10.1002/2015JD024480

Kitoh, A., Endo, H., Kumar, K. K., Cavalcanti, I. F. A., Goswami, P., & Zhou, T. (2013). Monsoons in a changing world: A regional perspective in a global context. *Journal of Geophysical Research: Atmospheres*, *118*, 3053–3065. https://doi.org/10.1002/jgrd.50258

Krishnamurthy, L., & Krishnamurthy, V. (2016). Teleconnections of Indian monsoon rainfall with AMO and Atlantic tripole. *Climate Dynamics*, *46*(7–8), 2269–2285. https://doi.org/10.1007/s00382-015-2701-3

Krishnan, R., Sabin, T. P., Ayantika, D. C., Kitoh, A., Sugi, M., Murakami, H., et al. (2013). Will the south Asian monsoon overturning circulation stabilize any further? *Climate Dynamics*, *40*(1–2), 187–211. https://doi.org/10.1007/s00382-012-1317-0

Lea, D. W., Shen, G. T., & Boyle, E. A. (1989). Coralline barium records temporal variability in equatorial Pacific upwelling. *Nature*, *340*(6232), 373–376. https://doi.org/10.1038/340373a0

McCulloch, M., Fallon, S., Wyndham, T., Hendy, E., Lough, J., & Barnes, D. (2003). Coral record of increased sediment flux to the inner great barrier reef since European settlement. *Nature*, *421*(6924), 727–730. https://doi.org/10.1038/nature01361

Naidu, C. V., Raju, A. D., Satyanarayana, G. C., Kumar, P. V., Chiranjeevi, G., & Suchitra, P. (2015). An observational evidence of decrease in Indian summer monsoon rainfall in the recent three decades of global warming era. *Global and Planetary Change*, *127*, 91–102. https://doi.org/10.1016/j.gloplacha.2015.01.010

Roxy, M. K., Ritika, K., Terray, P., Murtugudde, R., Ashok, K., & Goswami, B. N. (2015). Drying of Indian subcontinent by rapid Indian Ocean warming and a weakening land-sea thermal gradient. *Nature Communications*, *6*(1). https://doi.org/10.1038/ncomms8423

Shen, G. T., & Boyle, E. A. (1988). Determination of lead, cadmium and other trace metals in annually-banded corals. *Chemical Geology*, *67*(1–2), 47–62. https://doi.org/10.1016/0009-2541(88)90005-8

Shukla, J., & Misra, B. M. (1977). Relationships between sea-surface temperature and wind speed over central Arabian Sea, and monsoon rainfall over India. *Monthly Weather Review*, *105*(8), 998–1002. https://doi.org/10.1175/1520-0493(1977)105<0998:RBSSTA>2.0.CO;2

Sinha, A., Kathayat, G., Cheng, H., Breitenbach, S. F. M., Berkelhammer, M., Mudelsee, M., et al. (2015). Trends and oscillations in the Indian summer monsoon rainfall over the last two millennia. *Nature Communications*, *6*(1). https://doi.org/10.1038/ncomms7309

Sutton, R. T., Dong, B., & Gregory, J. M. (2007). Land/sea warming ratio in response to climate change: IPCC AR4 model results and comparison with observations. *Geophysical Research Letters*, *34*, L02701. https://doi.org/10.1029/2006GL028164

Tokinaga, H., Xie, S.-P., Deser, C., Kosaka, Y., & Okumura, Y. M. (2012). Slowdown of the Walker circulation driven by tropical indo-Pacific warming. *Nature*, *491*(7424), 439–443. https://doi.org/10.1038/nature11576

Torrence, C., & Compo, G. P. (1998). A practical guide to wavelet analysis. *Bulletin of the American Meteorological Society*, *79*(1), 61–78. https://doi.org/10.1175/1520-0477(1998)079<0061:APGTWA>2.0.CO;2

Turner, A. G., & Annamalai, H. (2012). Climate change and the South Asian summer monsoon. *Nature Climate Change*, *2*(8), 587–595. https://doi.org/10.1038/nclimate1495

Vareed Joseph, P., Gokulapalan, B., Nair, A., & Sheela Wilson, S. (2013). Variability of summer monsoon rainfall in India on inter-annual and decadal time scales. *Atmospheric and Oceanic Science Letters*, *6*(5), 398–403. https://doi.org/10.3878/j.issn.1674-2834.13.0044

Wang, B., Wu, R., & Lau, K.-M. (2001). Interannual variability of Asian summer monsoon: Contrast between the Indian and western North Pacific-East Asian monsoons. *Journal of Climate*, *14*(20), 4073–4090. https://doi.org/10.1175/1520-0442(2001)014<4073:IVOTAS>2.0.CO;2

Wang, B., Liu, J., Kim, H.-J., Webster, P. J., Yim, S.-Y., & Xiang, B. (2013). Northern hemisphere summer monsoon intensified by mega-El Nino/Southern Oscillation and Atlantic multidecadal oscillation. *Proceedings of the National Academy of Sciences of the United States of America*, *110*(14), 5347–5352. https://doi.org/10.1073/pnas.1219405110

Webster, P., Magana, V., Palmer, T., Shukla, J., Tomas, R., Yanai, M., & Yasunari, T. (1998). Monsoons: Processes, predictability, and the prospects for prediction. *Journal of Geophysical Research*, *103*(C7), 14,451–14,510. https://doi.org/10.1029/97JC02719

Wu, G., Liu, Y., He, B., Bao, Q., Duan, A., & Jin, F.-F. (2012). Thermal controls on the Asian summer monsoon. *Scientific Reports*, *2*(1). https://doi.org/10.1038/srep00404

Zhai, Ping. (2011). The response of the Red Sea to a strong wind jet near the Tokar Gap in summer (Master of Science). Woods Hole Oceanographic Institution and Massachusetts Institute of Technology. Retrieved from https://hdl.handle.net/1912/4836

Zhang, R., & Delworth, T. L. (2006). Impact of Atlantic multidecadal oscillations on India/Sahel rainfall and Atlantic hurricanes. *Geophysical Research Letters*, *33*, L17712. https://doi.org/10.1029/2006GL026267

Zhou, T., Zhang, L., & Li, H. (2008). Changes in global land monsoon area and total rainfall accumulation over the last half century. *Geophysical Research Letters*, *35*, L16707. https://doi.org/10.1029/2008GL034881

References From the Supporting Information

Murty, S. A. (2012). Centennial-scale climate variability from spatial SST gradients in Red Sea corals (Thesis).

Thomson, D. J. (1990). Time series analysis of Holocene climate data. *Philosophical Transactions. Royal Society of London*, *330*(1615), 601–616. https://doi.org/10.1098/rsta.1990.0041

Walden, A. T., McCoy, E., & Percival, D. B. (1994). The variance of multitaper spectrum estimates for real Gaussian processes. *IEEE Transactions on Signal Processing*, *42*(2), 479–482. https://doi.org/10.1109/78.275635